Fluid Dynamics & Materials Processing
DOI:10.32604/fdmp.2020.09666
Article

Tech Science Press

Effects of Wall Emissivity on Aerodynamic Heating in Scramjets

Yue Zhou[1] and Pengfei Ju[2,3,*]

[1]School of Aeronautical Science and Technology, Beihang University, Beijing, 100191, China
[2]Tianjin Key Laboratory for Advanced Mechatronic System Design and Intelligent Control, School of Mechanical Engineering, Tianjin University of Technology, Tianjin, 300384, China
[3]National Demonstration Center for Experimental Mechanical and Electrical Engineering Education (Tianjin University of Technology), Tianjin, 300384, China
[*]Corresponding Author: Pengfei Ju. Email: jupengfei_tjut@126.com
Received: 14 January 2020; Accepted: 23 April 2020

Abstract: The effects of the wall emissivity on aerodynamic heating in a scramjet are analyzed. The supersonic turbulent combustion flow including radiation is solved in the framework of a decoupled strategy where the flow field is determined first and the radiation field next. In particular, a finite difference method is used for solving the flow while a DOM (iscrete ordinates method) approach combined with a WSGGM (weighted sum of gray gases) model is implemented for radiative transfer. Supersonic nonreactive turbulent channel flows are examined for a DLR hydrogen fueled scramjet changing parametrically the wall emissivity. The results indicate that the wall radiative heating rises greatly with increasing the wall emissivity. As the wall emissivity rises, the radiative source and total absorption increase, while the incident radiation decreases apparently. Notably, although the radiative heating can reach a significant level, its contribution to the total aerodynamic heating is relatively limited.

Keywords: Scramjet; aerodynamic heating; wall emissivity; radiation

1 Introduction

Aerodynamic heating is an important and difficult issue in scramjet research, influenced by plenty of complicated physical and chemical phenomena, such as high-speed jet, shock waves, combustion reactions, and thermal radiation, etc. Among the above various complex processes, radiation has attracted more and more attention recently. Nelson [1] simulated the chemically reacting flow fields in supersonic combustor models coupled with a one-dimensional radiative heat transfer solution, which showed that the radiative heating was amount roughly 10% of the convective heating. Surzhikov et al. [2] predicted both the convective and radiative heating of internal surfaces in a dual-mode scramjet model and the NASA SCHOLAR scramjet model, respectively, by NERAT-2D code, which demonstrated that the radiative heating contributed significantly to the total heating of the combustor wall. Their quasi-one-dimensional model was then validated by comparison with several experiments [3]. Wang et al. [4] developed a decoupled procedure to compute the turbulent combustion flows including radiation in DLR hydrogen fueled and SCHLOAR ethylene fueled scramjets, respectively, which indicated that radiative heating reached an order of 10 kW/m^2, but not greater than 7% of convective heating. Other similar researches

are referred to [5]. However, research on thermal radiation in the scramjet is still much immature, which needs more thorough works.

The paper mainly discusses the emissivity effects on aerodynamic heating, particularly radiative heating, in scramjet, by a decoupled simulation strategy developed by Wang et al. [4], combing finite difference code for flow field and discrete ordinates method (DOM) for radiative transfer including an weighted sum of gray gases model (WSGGM) for spectral property calculation. Firstly, a series of supersonic nonreactive turbulent channel flow cases with different wall emissivities are conducted for detailed parametric studies. Then, as an application situation, the flow field including radiation in DLR hydrogen fueled scramjet is simulated, in which the wall emissivity effects are investigated meticulously.

2 Mathematical and Physical Models

2.1 Governing Equations

The conservation forms of Navier-Stokes equations including chemical reactions are as follows:

$$\begin{cases} \dfrac{\partial(\rho Y_s)}{\partial t}+\dfrac{\partial\left(\rho Y_s u_j\right)}{\partial x_j}=\dfrac{\partial}{\partial x_j}\left(\rho D_s\dfrac{\partial Y_s}{\partial x_j}\right)+\omega_s, s=1,2,\cdots,ns \\ \dfrac{\partial(\rho u_i)}{\partial t}+\dfrac{\partial\left(\rho u_i u_j+p\delta_{ij}\right)}{\partial x_j}=\dfrac{\partial\tau_{ij}}{\partial x_j} \\ \dfrac{\partial(\rho E)}{\partial t}+\dfrac{\partial\left(\rho H u_j\right)}{\partial x_j}=\dfrac{\partial}{\partial x_j}\left(\tau_{ij}u_i+k\dfrac{\partial T}{\partial x_j}+\sum_{s=1}^{ns}\rho D_s h_s\dfrac{\partial Y_s}{\partial x_j}-q_{rj}\right) \end{cases} \tag{1}$$

where ρ, u_i, p and T are density, velocity in i-direction, pressure and temperature, respectively; τ_{ij} is the shear stress tensor, and δ_{ij} is Kronecker function; E and H are respectively total energy and enthalpy per unit volume; ns is total number of species; D_s, h_s and $\omega_s$are mass diffusion coefficient, absolute enthalpy per unit mass and mass production rate per unit volume of species s; q_{rj} is the radiative heat flux. In the current research, Favrè average is introduced to Eq. (1) and the Menter's k-ω SST two-equation model [6] including the compressible correction [7] is selected for the turbulence closure.

Assuming the local thermodynamic equilibrium exists and ignoring the scattering effects of radiative participants, radiative transfer equation follows:

$$\mu_i\frac{\partial I_v(\boldsymbol{r},\boldsymbol{\mu})}{\partial x_i}=\kappa_v[I_{bv}(\boldsymbol{r})-I_v(\boldsymbol{r},\boldsymbol{\mu})] \tag{2}$$

where the subscript 'v' is radiation frequency; $\boldsymbol{r}$ denotes the spatial location and $\boldsymbol{\mu}$ represents a directional unit vector; κ_v, I_{bv} and I_v are, respectively, the spectral absorption coefficient, spectral blackbody radiation intensity and spectral radiation intensity. The radiative heat flux divergence is

$$\frac{\partial q_{rj}}{\partial x_j}=\int_0^\infty\kappa_v\left[4\pi I_{bv}(\boldsymbol{r})-\int_{4\pi}I_v(\boldsymbol{r},\boldsymbol{\mu})d\Omega\right]dv \tag{3}$$

The wall radiative heat flux is expressed as:

$$q_{rw}=\int_0^\infty\varepsilon_{wv}\left[\int_{\boldsymbol{n}_w\cdot\boldsymbol{B}<0}I_v(\boldsymbol{r}_w,\boldsymbol{\mu})|n_{wi}\mu_i|d\Omega-E_{bv}\right]dv \tag{4}$$

where ε_{wv} is the wall spectral emissivity; E_{bv} is the spectral blackbody emissive power; $\boldsymbol{n}_w$ denotes the unit vector normal at the wall.

2.2 Weighted Sum of Gray Gases Model

In the weighted sum of gray gases model [8] (WSGGM) for calculating the properties of radiation participating gases, the non-gray gas is replaced by several gray gases respectively with temperature independent absorption coefficients and temperature dependent weighted factors, whereas the overall radiative effect is regarded as a sum of the individual influences of the gray gases. The WSGGM has advantages in small calculation amount and adequate accuracy. In present study, Perry 5GG WSGGM proposed by Krishnamoorthy [9] for CO_2 and H_2O is used, in which the weighted factors for gray gases are linear functions of the temperature, and the absorption coefficients for gray gases are given by the pressure and the densities of CO_2 and H_2O. The weighted factors and the expressions of the absorption coefficients are taken from [9,10].

According to WSGGM, radiative transfer Eq. (2) is re-expressed as:

$$\begin{cases} \mu_i \dfrac{\partial I_k(\boldsymbol{r},\boldsymbol{\mu})}{\partial x_i} = \kappa_k \left[a_k \dfrac{\sigma T^4}{\pi} - I_k(\boldsymbol{r},\boldsymbol{\mu}) \right] \\ I(\boldsymbol{r},\boldsymbol{\mu}) = \sum\limits_{k=1}^{K} I_k(\boldsymbol{r},\boldsymbol{\mu}) \end{cases} \tag{5}$$

where K is the total number of gray gases; a_k and κ_k are the weighted factor and absorption coefficient of the k-th gray gas, respectively; T is the temperature and σ is the Stefan-Boltzmann constant. The radiative heat flux divergence is split as:

$$\begin{cases} \dfrac{\partial q_{rj,k}}{\partial x_j} = \kappa_k(\boldsymbol{r}) \left[4 a_k \sigma T^4(\boldsymbol{r}) - \displaystyle\int_{4\pi} I_k(\boldsymbol{r},\boldsymbol{\mu}) d\Omega \right] \\ \dfrac{\partial q_{rj}}{\partial x_j} = \displaystyle\sum_{k=1}^{K} \dfrac{\partial q_{rj,k}}{\partial x_j} \end{cases} \tag{6}$$

For diffusively gray wall, the wall radiative heat flux is

$$\begin{cases} q_{rw,k} = \varepsilon_w \left[\int_{\boldsymbol{n}_w \cdot \boldsymbol{B} < 0} I_k(\boldsymbol{r}_w,\boldsymbol{\mu}) |n_{wi}\mu_i| d\Omega - a_k \sigma T_w^4 \right] \\ q_{rw} = \displaystyle\sum_{k=1}^{K} q_{rw,k} \end{cases} \tag{7}$$

where ε_w and T_w are the wall emissivity and temperature, respectively.

3 Simulation Methods

3.1 Numerical Schemes

In present research, a numerical solver, developed by Gao et al. [11–14], is used for the supersonic turbulent combustion flow field simulation based on the finite difference method. In the solver, the Roe scheme is used for discretizing the convective flux vectors and the MUSCL method is introduced to achieve a second-order precision; a central difference is adopted to discretize the viscous terms, and the implicit LU-SGS method for the time integration.

The discrete ordinates method (DOM) [15], convenient to couple with the finite difference computation for the flow field, is employed for solving the RTE. Considering the accuracy and stability in solving process, S_4 and step schemes are, respectively, adopted for the angular quadrature and spatial discretization in DOM.

According to [4], a decoupled strategy for solving the supersonic turbulent combustion flow with radiation is utilized in present study: solve the supersonic turbulent combustion flow first without radiation to be convergent; then, the radiation field is computed based on the flow field data, details can be referred [4].

3.2 Grid Independence

A case of the generic direct-connect scramjet for hydrogen fuel of German Aerospace Center (DLR) [16] is used for discussing the grid independence of the present numerical schemes. The geometric sketch of the scramjet is shown in Fig. 1, in which the hydrogen is injected parallel to the air stream through the holes at the base of a wedge. The air flow and hydrogen jet conditions are listed in Tab. 1. Both the top and bottom walls are taken with the same temperature 400 K. It has been shown that the convective heating is very sensitive to the grid refinement and the initial grid spacing near the wall is of great significance [17]. Therefore, the convective heat flux at x = 0.0534 m on the bottom wall is selected as the supervised variable for discussing the grid independence. Four meshes are used to simulate the turbulent combustion flowfield in the DLR scramjet. The total numbers of grid nodes of these four meshes are 22740, 30320, 38500 (see Fig. 2) and 45480, respectively, with the corresponding initial grid spacing of 1×10^{-4} m, 1×10^{-5} m, 1×10^{-6} m and 5×10^{-7} m. Fig. 3 shows the effect of the grid refinement on the wall convective heat flux. The grid with 38500 nodes and the initial grid spacing of 1×10^{-6} m is refined enough to predict the convergent convective heating. According to this, for the later simulations, the initial grid spacing near the wall is set to be not greater than 1×10^{-6} m.

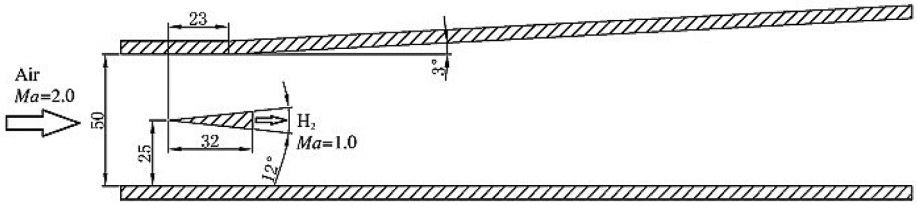

Figure 1: Geometric sketch of the DLR scramjet

Table 1: Conditions for air stream and H_2 jet in DLR scramjet

	Ma	T_∞/K	p_∞/Pa	Y_{H2}	Y_{O2}	Y_{H2O}	Y_{N2}
Air stream	2.0	340	10^5	0.0	0.232	0.032	0.736
H_2 jet	1.0	250	10^5	1.0	0.0	0.0	0.0

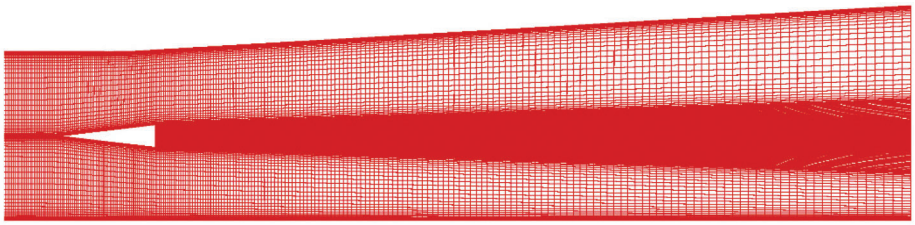

Figure 2: The CFD mesh for the DLR scramjet with the total number of grid nodes of 38500

3.3 Validation

The DLR scramjet case is still employed to validate the reliability of the present numerical schemes, since it has the experimental data of temperature for comparison. In this section, the grid of 38500 nodes is used and both the top and bottom walls of the DLR scramjet are set to be adiabatic. Fig. 4 compares the present results with the experimental temperature data [16] in the y-direction, respectively, at x = 61 mm and 216 mm, which shows a good agreement. Therefore, the present simulation solver is reliable.

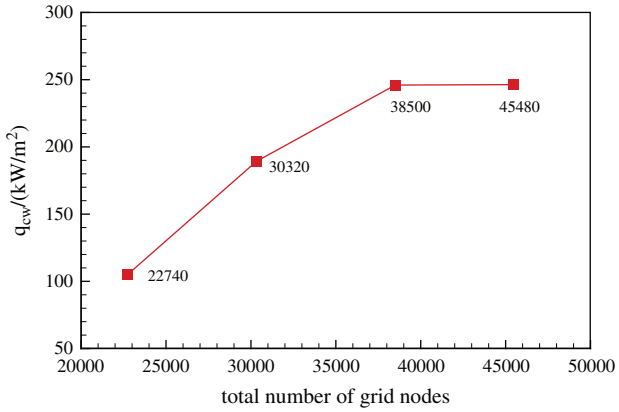

Figure 3: Effect of the grid refinement on the convective heating

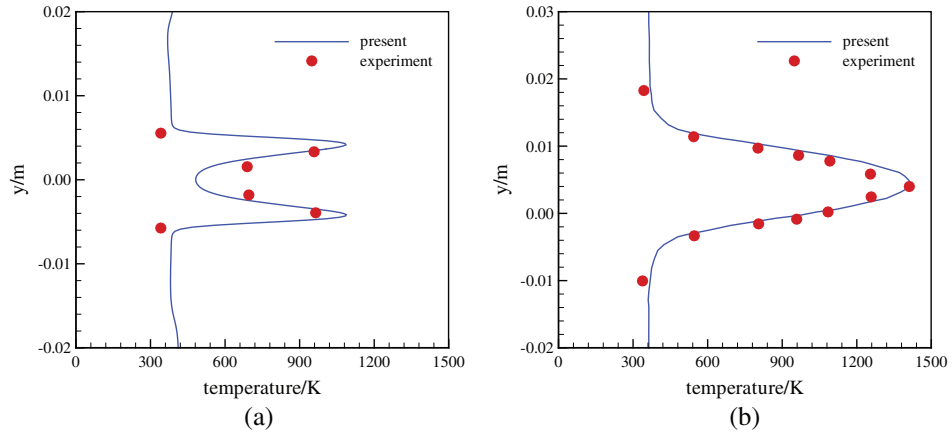

Figure 4: Comparison of the present results with the experimental temperature data in the y-direction at two x-locations. (a) x = 0.061 m and (b) x = 0.216 m

Since this paper focuses on the heat transfer behavior, simulation results in the present paper don't include flow parameter distributions, which are often discussed in supersonic ejectors [18].

4 Results

4.1 Supersonic Turbulent Channel Flows

A series of supersonic nonreactive turbulent channel flow cases are computed for parametric studies on the wall emissivity effects. The rectangular channel with dimensions of 1.0 m × 0.2 m is sketched in Fig. 5, and between the two walls is filled with fully radiative participants of CO_2 and H_2O. Assume both the top and bottom walls are diffusive and gray with the same emissivity. In all simulations, Ma = 2.0, ρ_∞ = 1.0 kg/m^3, T_∞ = 2000 K, the wall temperature T_w = 300 K, the CO_2 mass fraction Y_{CO2} = 0.5, the stream turbulence intensity is given as 1%, and the wall emissivity ε = 0.2, 0.4, 0.6, 0.8, 1.0, respectively. The specific heat and enthalpy of CO_2 and H_2O are expressed in temperature-fitted polynomials [19]. The simulation grids are 80 × 100, and the first point distance from the wall is taken as 1.0 × 10^{-7} m to keep adequate precision on predicting aerodynamic heating.

Figs. 6a and 6b shows the convective heating and radiative heating variations with different ε along streamwise direction. Due to the fact that radiation nearly has no influence on the flow field, there is only one curve for the convective heating in Fig. 6a. Both convective and radiative heat fluxes decrease

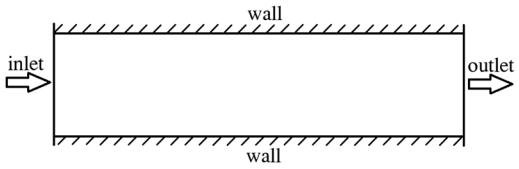

Figure 5: The supersonic nonreactive turbulent channel

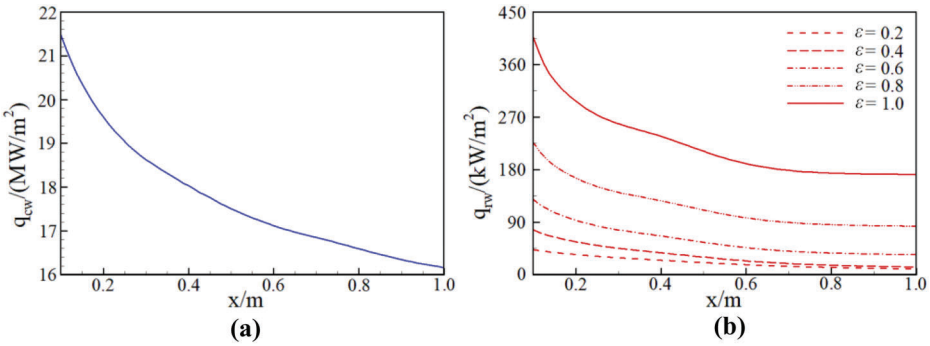

Figure 6: Aerodynamic heating varing with ε along x-axis. (a) Convective heating q_{cw} and (b) Radiative heating q_{rw}

streamwisely. The boundary layer thickens gradually along x-axis. The temperature gradient declines in the boundary layer to reduce the convective heating, while the low temperature region extends to weaken the radiative heating. Fig. 6 also shows that the radiative heating is only a small percent of the convective heating (<2%).

Fig. 6b demonstrates that the radiative heating rises as the wall emissivity increases, which can be seen more clearly in Fig. 7. Fig. 7 displays the radiative heating at different x stations, x = 0.25, 0.50, 0.75 m, respectively. It shows that the radiative heating increases dramatically with ε rising. The emissivity effects on the radiative heating can be deduced from Eqs. (4) or (7). Although there is a formally linear relation between the radiative heating and the wall emissivity in Eqs. (4) or (7), the results actually appear nearly exponential for the reason that the wall emissivity ε can also affect the radiation intensity greatly.

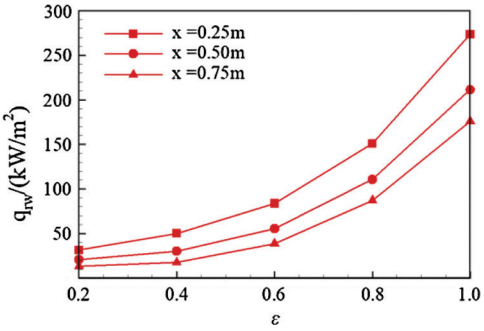

Figure 7: Effects of wall emissivity on radiative heating

4.2 DLR Hydrogen Fueled Scramjet

The wall emissivity effects are also investigated in the DLR scramjet case as an application situation. Both the top and bottom walls are taken the same wall emissivity ε = 0.2, 0.4, 0.6, 0.8, 1.0. The total number of simulation grids is about 38,500, and the distance of the first layer of the mesh next to the

wall is 1×10^{-6} m. The chemical dynamic model for hydrogen/air reaction including 7 species and 8 elemental reactions from [20] is chosen, and temperature-fitted polynomials coefficients of specific capacities and enthalpies of all reactants from [19] are used.

Figs. 8–12 depict, respectively, the distributions of the temperature, H_2O mass fraction, radiative source (the minus divergence of the radiative heat flux), total absorption coefficient and incident radiation in DLR scramjet with $\varepsilon = 0.8$. The total absorption coefficient and incident radiation respectively follow:

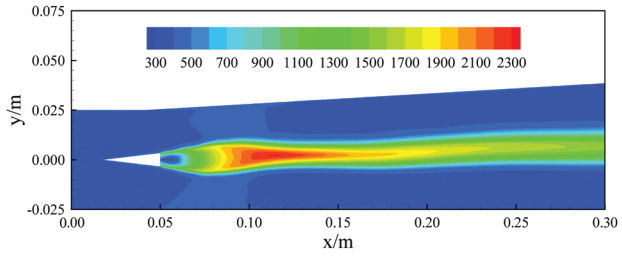

Figure 8: Temperature distribution in DLR scramjet with $\varepsilon = 0.8$

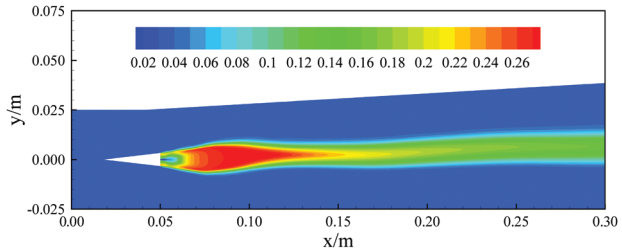

Figure 9: H_2O mass fraction distribution in DLR scramjet with $\varepsilon = 0.8$

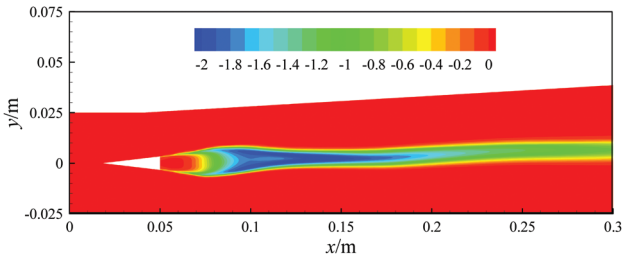

Figure 10: Radiative source distribution in DLR scramjet with $\varepsilon = 0.8$

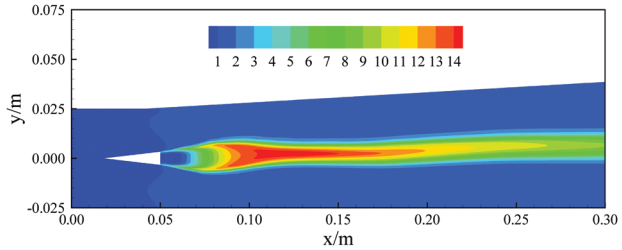

Figure 11: Total absorption coefficient distribution in DLR scramjet with $\varepsilon = 0.8$

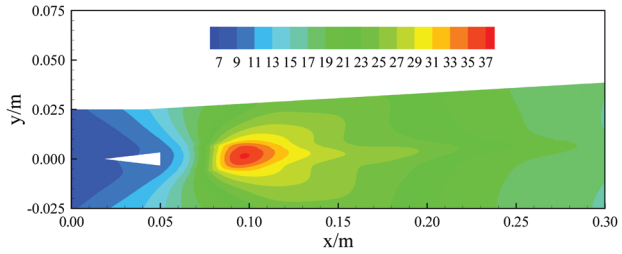

Figure 12: Incident radiation distribution in DLR scramjet with $\varepsilon = 0.8$

$$\kappa = \frac{\int_0^\infty \left(\int_{4\pi} \kappa_v I_v d\Omega\right) dv}{\int_0^\infty \left(\int_{4\pi} I_v d\Omega\right) dv} \tag{8}$$

$$G = \int_0^\infty \left(\int_{4\pi} I_v d\Omega\right) dv \tag{9}$$

Figs. 8–12 indicate that, generally, the higher the temperature and H_2O mass fraction are, the greater the radiative source, total absorption coefficient, and the incident radiation are. It also demonstrates that the spatial distributions of the radiative source and total absorption coefficient are highly in consistent with those of the temperature and radiative participants (H_2O), while the spatial distribution of the incident radiation spreads wider. Similar results can be found in other ε situations as well.

Figs. 13–15 show the variations of the radiative source, total absorption and incident radiation as the different wall emissivity at three x stations in DLR scramjet, respectively. Figs. 13–15 indicate that as the wall emissivity increases, the radiative source (absolute value) and total absorption coefficient rise, while the incident radiation decreases apparently.

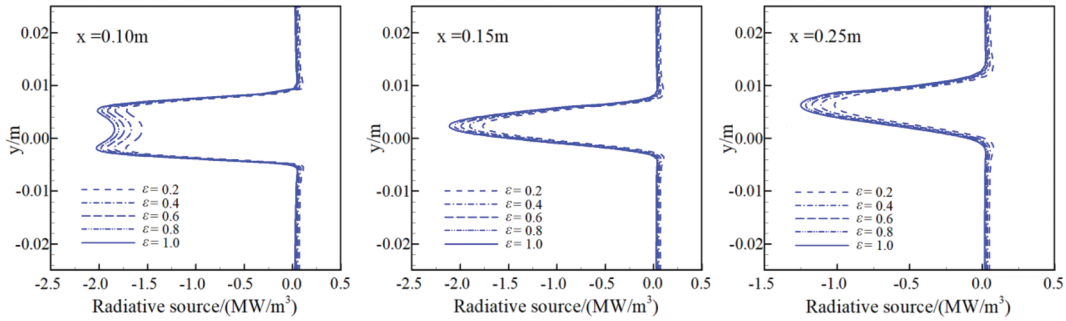

Figure 13: Effects of wall emissivity on the radiative source. (a) $x = 0.10$ m (b) $x = 0.15$ m and (c) $x = 0.25$ m

Fig. 16 depicts the convective heating and radiative heating both at the top and bottom wall in DLR scramjet with different wall emissivities, ε = 0.2, 0.4, 0.6, 0.8, 1.0. Since the radiation nearly has no effects on the flow field, there is only one result for the convective heating, with a peak of about 250 kW/m^2. The radiative heating goes up with the increasing ε, which can be clearly drawn from Eqs. (4) or (7), and there exists a peak of about 6.7 kW/m^2 as ε = 1.0. The results also show that although the radiative heating can reach an order of 10 kW/m^2, it still contributes very little to the total aerodynamic heating.

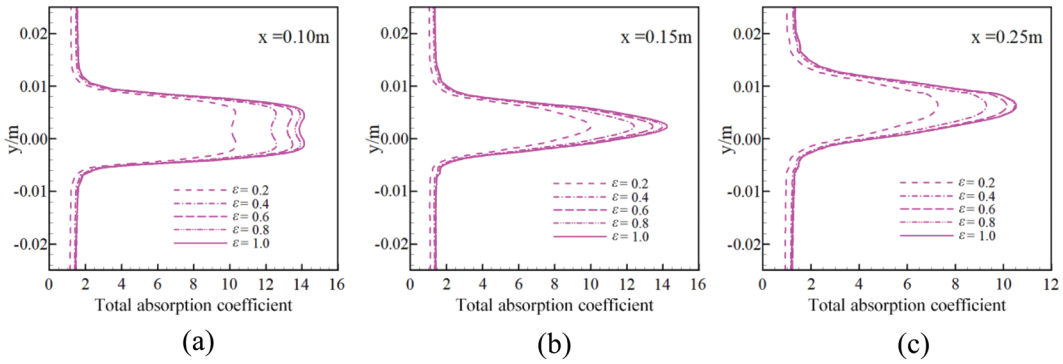

Figure 14: Effects of wall emissivity on the total absorption coefficient. (a) $x = 0.10$ m (b) $x = 0.15$ m and (c) $x = 0.25$ m

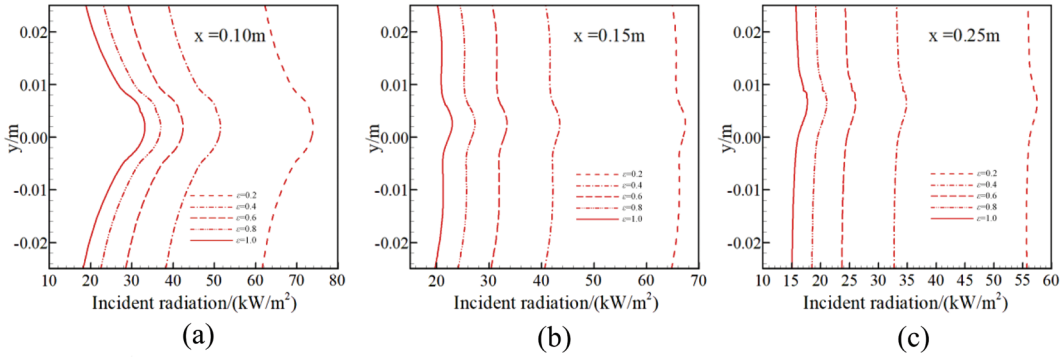

Figure 15: Effects of wall emissivity on incident radiation. (a) $x = 0.10$ m (b) $x = 0.15$ m and (c) $x = 0.25$ m

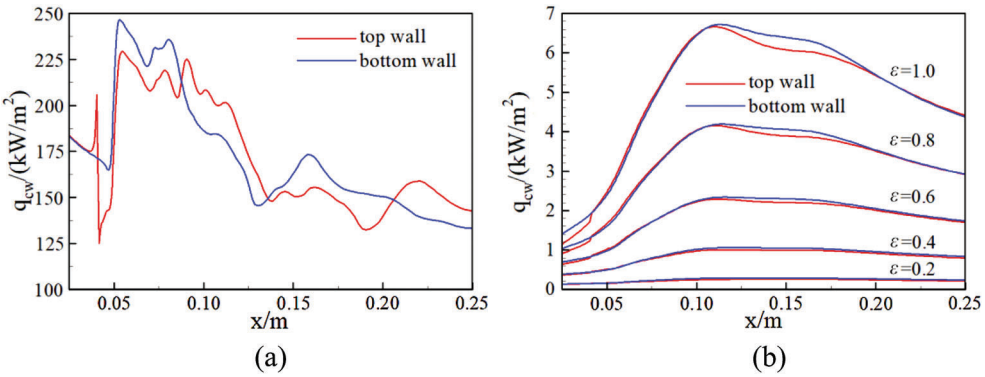

Figure 16: Aerodynamic heating in DLR hydrogen fueled scramjet varying with ε. (a) Convective heating q_{cw} and (b) Radiative heating q_{rw}

5 Conclusion

In present research, the wall emissivity effects on aerodynamic heating in scramjet are investigated. The supersonic turbulent combustion flow including radiation is solved by a decoupled procedure that computes flow field first and radiation field next, in which the finite difference method is used for solving flow and DOM conjugated with WSGGM for radiative transfer.

Supersonic nonreactive turbulent channel flows and DLR hydrogen fueled scramjet with different wall emissivities, are simulated respectively for parametric and application studies. The results indicate that the radiative heating will rise greatly with the increasing ε. In DLR scramjet, as the wall emissivity rises, the radiative source and total absorption increase, while the incident radiation decreases apparently. Besides, although the radiative heating can reach a certain level, it still contributes very little to total aerodynamic heating.

Funding Statement: The authors received no specific funding for this study.

Conflicts of Interest: The authors declare that they have no conflicts of interest to report regarding the present study.

References

1. Nelson, H. F. (1997). Radiative heating in scramjet combustors. *Journal of Thermophysics and Heat Transfer, 11 (1),* 59–64. DOI 10.2514/2.6201.
2. Surzhikov, S. T., Zheleznyakova, A. L., Shang, J. S., Rivir, R. B. (2013). Simulating gasdynamic interaction and radiative heating within scramjets with hydrocarbon fuels. *44th AIAA Thermophysics Conference*, *San Diego, CA*.
3. Surzhikov, S. T., Seleznev, R. K. (2015). Quasi-one-dimensional and two-dimensional numerical simulation of scramjet combustors. *51st AIAA/SAE/ASEE Joint Propulsion Conference*, *Orlando, FL*.
4. Wang, J. Y., Gao, Z. X., Lee, C. H., Zhang, H. Q. (2014). A decoupled procedure for convection-radiation simulation in scramjets. *Science China Technological Sciences, 57(12),* 2551–2566. DOI 10.1007/s11431-014-5706-y.
5. Seleznev, R. K., Surzhikov, S. T., Shang, J. S. (2019). A review of the scramjet experimental data base. *Progress in Aerospace Sciences, 106,* 43–70. DOI 10.1016/j.paerosci.2019.02.001.
6. Menter, F. R. (1994). Two-equation eddy-viscosity turbulence models for engineering applications. *AIAA Journal, 32(8),* 1598–1605. DOI 10.2514/3.12149.
7. Wilcox, D. C. (1998). *Turbulence Modeling for CFD*. La Canada, USA: DCW industries.
8. Hottel, H. C., Sarofim, A. F. (1967). *Radiative Transfer*. New York, USA: McGraw-Hill.
9. Krishnamoorthy, G. (2010). A new weighted-sum-of-gray-gases model for CO_2–H_2O gas mixtures. *International Communications in Heat and Mass Transfer, 37(9),* 1182–1186. DOI 10.1016/j.icheatmasstransfer.2010.07.007.
10. Edwards, D. K., Matavosian, R. (1984). Scaling rules for total absorptivity and emissivity of gases. *Journal of Heat Transfer, 106(4),* 684–689. DOI 10.1115/1.3246739.
11. Gao, Z. X., Lee, C. H. (2010). A numerical study of turbulent combustion characteristics in a combustion chamber of a scramjet engine. *Science China Technological Sciences, 53(8),* 2111–2121. DOI 10.1007/s11431-010-3088-3.
12. Li, J., Lee, C. H., Jia, L., Li, X. (2009). Numerical study on flow control by micro-blowing. *47th AIAA Aerospace Sciences Meeting Including the New Horizons Forum and Aerospace Exposition*, *Orlando, FL*.
13. Gao, Z. X., Lee, C. H. (2010). A flamelet model for turbulent diffusion combustion in supersonic flow. *Science China Technological Sciences, 53(12),* 3379–3388. DOI 10.1007/s11431-010-4169-z.
14. Gao, Z. X., Jiang, C. W., Lee, C. H. (2013). Improvement and application of wall function boundary condition for high-speed compressible flows. *Science China Technological Sciences, 56(10),* 2501–2515. DOI 10.1007/s11431-013-5349-4.
15. Modest, M. F. (2003). *Radiative heat transfer*. San Diego: Academic Press.
16. Oevermann, M. (2000). Numerical investigation of turbulent hydrogen combustion in a SCRAMJET using flamelet modeling. *Aerospace Science and Technology, 4(7),* 463–480. DOI 10.1016/S1270-9638(00)01070-1.
17. Bertin, J. J., Cummings, R. M. (2006). Critical hypersonic aerothermodynamic phenomena. *Annual Review of Fluid Mechanics, 38(1),* 129–157. DOI 10.1146/annurev.fluid.38.050304.092041.
18. Dandani, M., Lepiller, V., Ghezal, A., Desevaux, P. (2018). Numerical visualizations of mixing enhancement in a 2D supersonic ejector. *Fluid Dynamics & Materials Processing, 14(1),* 23–37.

19. Kee, R. J., Rupley, F. M., Miller, J. A. (1990). *The chemkin thermodynamic data base (No. SAND-87-8215B)*. Livermore, CA, USA: Sandia National Labs.
20. Spiegler, E., Wolfshtein, M., Manheimer-Timnat, Y. (1976). A model of unmixedness for turbulent reacting flows. *Acta Astronautica, 3(3–4),* 265–280. DOI 10.1016/0094-5765(76)90051-5.